

Article

Intra-Amniotic Administration—An Emerging Method to Investigate Necrotizing Enterocolitis, In Vivo (*Gallus gallus*)

Nikolai Kolba , Jacquelyn Cheng , Cydney D. Jackson  and Elad Tako *

Department of Food Science, Cornell University, Stocking Hall, Ithaca, NY 14850, USA

* Correspondence: et79@cornell.edu; Tel.: +1-607-255-0884

Abstract: Necrotizing enterocolitis (NEC) is a severe gastrointestinal disease in premature infants and a leading cause of death in neonates (1–7% in the US). NEC is caused by opportunistic bacteria, which cause gut dysbiosis and inflammation and ultimately result in intestinal necrosis. Previous studies have utilized the rodent and pig models to mimic NEC, whereas the current study uses the in vivo (*Gallus gallus*) intra-amniotic administration approach to investigate NEC. On incubation day 17, broiler chicken (*Gallus gallus*) viable embryos were injected intra-amniotically with 1 mL dextran sodium sulfate (DSS) in H₂O. Four treatment groups (0.1%, 0.25%, 0.5%, and 0.75% DSS) and two controls (H₂O/non-injected controls) were administered. We observed a significant increase in intestinal permeability and negative intestinal morphological changes, specifically, decreased villus surface area and goblet cell diameter in the 0.50% and 0.75% DSS groups. Furthermore, there was a significant increase in pathogenic bacterial (*E. coli* spp. and *Klebsiella* spp.) abundances in the 0.75% DSS group compared to the control groups, demonstrating cecal microbiota dysbiosis. These results demonstrate significant physiopathology of NEC and negative bacterial–host interactions within a premature gastrointestinal system. Our present study demonstrates a novel model of NEC through intra-amniotic administration to study the effects of NEC on intestinal functionality, morphology, and gut microbiota in vivo.



Citation: Kolba, N.; Cheng, J.; Jackson, C.D.; Tako, E. Intra-Amniotic Administration—An Emerging Method to Investigate Necrotizing Enterocolitis, In Vivo (*Gallus gallus*). *Nutrients* **2022**, *14*, 4795. <https://doi.org/10.3390/nu14224795>

Academic Editor: Rosa Casas

Received: 11 October 2022

Accepted: 8 November 2022

Published: 12 November 2022

Publisher's Note: MDPI stays neutral with regard to jurisdictional claims in published maps and institutional affiliations.



Copyright: © 2022 by the authors. Licensee MDPI, Basel, Switzerland. This article is an open access article distributed under the terms and conditions of the Creative Commons Attribution (CC BY) license (<https://creativecommons.org/licenses/by/4.0/>).

Keywords: necrotizing enterocolitis; NEC; dextran sodium sulfate; intraamniotic administration; *Gallus gallus*; gut microbiome; dysbiosis; intestinal immaturity

1. Introduction

In premature infants, a leading gastrointestinal disease, necrotizing enterocolitis (NEC), accounts for approximately 2–13% of preterm and very-low-birth-weight (VLBW, <1500 g) infants in the United States [1–3]. Variations in incidences are attributed to different risk factor profiles, such as differing populations, detection rates, and inclusion and exclusion criteria for the disease [4–7]. Currently, there is no global incidental rate on NEC. Previous literature suggests that NEC is caused by intra-luminal pathogenic bacteria disrupting the intestinal villi, which upregulates inflammatory pathways, causing dysbiosis, and ultimately results in intestinal necrosis [8–10]. NEC is a multifactorial disease wherein symptoms start slowly, but decompensation occurs quickly, leading to fulminate NEC with pneumatosis intestinalis and portal gases [11–14]. The bacterial endotoxins released from opportunistic bacteria bind to Toll-like receptor four within epithelial cells, which activate pathogen-associated molecular pattern (PAMP) and release a complement and coagulation cascade effect within the immune system to break down gut mucosa [15–17]. Intestinal barrier disruption leads to bacteria entering intestinal cells and causes possible ischemia–reperfusion injury to the tissue [18].

NEC was initially investigated and induced in rodent and pig models through hypoxic/hypothermic and/or surgical interventions to mimic the multifactorial nature of the human disease [6,19–21]. In 1974, Barlow et al. demonstrated the first NEC model in rats, where gut flora and lack of immunoglobulin A (IgA) from breast milk were found to be

essential factors contributing to NEC-like injury [22]. Currently, model organisms for NEC include rodents, pigs, and gnotobiotic quail, each with distinct strengths and weaknesses in modeling NEC [23,24]. Rats modeling NEC have practical benefits such as a low cost and high resilience to stress compared with mice; however, rats lack biomolecular reagents such as antibodies, meaning specific genetic techniques cannot be utilized to understand the mechanisms of pathophysiology, unlike mice [24]. The mouse model has been used to demonstrate NEC prevention mechanisms but is limited, as reproducible data is not necessarily obtained [19,25–27]. Another model, pigs, which have a closer resemblance in size, physiology, and anatomy when compared to a premature infant [28–30], is costly to maintain, and genetic techniques are limited [20,31–33]. Additionally, piglet models utilize intestinal injury to induce NEC, affecting the whole GI tract, while human NEC occurs primarily in the distal small intestine [32]. Lastly, there is the quail model, which is practical for NEC because of their modest size; rapid, productive maturation; resilience to research manipulation; transgenic lines; fully sequenced genome; and availability for molecular manipulation [34–37].

The current study suggests an alternative and novel model for NEC, the chicken (*Gallus gallus*). The chicken has been a well-studied model organism since the last century due to genetic analysis in developmental biology, virology, oncology, and immunology [38]. Chickens have been utilized for several human diseases, including muscular dystrophy [39–41], bacterial infections [42–45], autoimmunity [46–48], cancer [49–51], the microbiome [52–57], and micronutrient deficiencies [58–64]. The external embryology of the chicken has been a leading system investigating vertebrate development using functional genomics and biochemistry to study diseases similar to NEC. We hypothesize that the intra-amniotic administration [64–66] of dextran sulfate sodium (DSS, a compound previously demonstrated to induce NEC) will lead to NEC development, causing clinical symptoms within the brush border membrane functionality, tissue morphology, and dysbiosis of the intestinal microbial populations.

2. Materials and Methods

2.1. Sample Preparation

Dextran sulfate sodium (>98%) (Catalog #J62101.14, molecular weight 165.19 g/mol, ThermoFisher, Waltham, MA, USA) was used for the intra-amniotic administration experiment. In addition, 4 kDa fluorescein isothiocyanate-dextran (FITC-Dextran, Catalog #SIAL-46944-100M, Sigma-Aldrich, St. Louis, MO, USA) was used for the intestinal permeability assay.

2.2. Animals and Study Design

Cornish cross-fertile broiler eggs ($n = 59$) were purchased from a hatchery (Moyer's Chicks, Quakertown, PA, USA). The eggs were incubated under standard conditions at the Cornell University Animal Science poultry farm. All animal experiments were approved and performed in compliance with Cornell University IACUC (protocol code: 2020-0077).

Intra-Amniotic Administration

Pure DSS solutions were individually diluted in deionized (DI) water. As previously described [54,56,61–63,67], intra-amniotic administration was completed on day 17 of embryonic development with viable embryos ($n = 60$). Eggs were weighed and divided into six treatment groups of equal weight distribution ($n = 10$), using a random sequence generation [68]. For the intra-amniotic administration, all eggs were disinfected by spraying 70% ethanol. In the H₂O control and DSS-treated groups, a 21-gauge needle was inserted into the amniotic fluid, and 1 mL of sterile solution was injected. The site for intra-amniotic administration was identified via candling. After the administration, the injection sites were sprayed with 70% ethanol and sealed with transparent tape. The eggs were distributed into six groups: (1) no injection, (2) DI H₂O, (3) 0.10% DSS, (4) 0.25% DSS, (5) 0.50% DSS, and (6) 0.75% DSS. The eggs were equally distributed in each incubator to reduce possible

allocation bias. Upon hatch, on incubation day 21, chicks were euthanized by CO₂. The blood was obtained via cardiac puncture and stored at 4 °C, then fractionated and stored at −20 °C. The proventriculus, gizzard, liver, pectoral muscle, duodenum, and cecum were obtained, flash frozen in liquid nitrogen, and stored at −20 °C until analysis.

2.3. Intestinal Permeability Test: Fluorescein Isothiocyanate Dextran (FITC-Dextran) Test

The intestinal permeability of the hatchlings was determined on day of hatch, as previously described by Barekatin et al., 2019 [69]. Briefly, on the day of hatch, each bird was orally gavaged with a 0.5 mL aqueous solution containing 1.1 mg of fluorescein isothiocyanate dextran (FITC-Dextran) before euthanization. A blood sample was taken from each bird after 4 h via myocardial puncture. Blood samples were fractionated via centrifugation at 1000× g for 15 min (Allegra X-30R, Beckman Coulter, Brea, CA, USA) and kept at −20 °C until analysis. Plasma samples and standards were analyzed in triplicate for FITC-Dextran concentration using a Biotek Epoch Microplate Spectrophotometer (Agilent Technologies, Santa Clara, CA, USA) with excitation and emission wavelengths set at 485 and 530 nm, respectively.

2.4. Glycogen Analysis as a Measurement of Energetic Status

All procedures were conducted as previously described [54,56,70]. A total of 20 mg of the liver was collected for glycogen analysis. Hepatic glycogen content was determined by multiplying the weight of the tissue by the amount of glycogen per 1 g of wet tissue.

2.5. Isolation of the Total RNA from the Duodenum Samples

As previously described [54,56,67], a RNeasy Mini Kit (Catalog #74106, Qiagen Inc., Valencia, CA, USA) utilized 30 mg of duodenal tissue ($n = 5$) to extract the total RNA according to the manufacturer's protocol. Total RNA was eluted in 50 µL of RNase-free water. All steps were carried out under RNase-free conditions. RNA was quantified by absorbance at 260/280 nm, and the integrity of the RNA was verified by 1.5% agarose gel electrophoresis followed by ethidium bromide staining. RNA was stored at −80 °C.

2.6. Real-Time Polymerase Chain Reaction (RT-PCR)

To create the cDNA, a 20 µL reverse transcriptase (RT) reaction was completed in a BioRad CFX1000 Touch thermocycler (BioRad, Hercules, CA, USA) using the Improm-II Reverse Transcriptase Kit (Catalog #A1250; Promega, Madison, WI, USA). The concentration of the cDNA obtained was determined by measuring the absorbance at 260/280 nm with an extinction coefficient of 33 (single-stranded DNA) by a NanoDrop 1000 Spectrophotometer (ThermoFisher Scientific, Waltham, MA USA). A RT-PCR assay assessed genomic DNA contamination for the genetic samples [67,71].

2.7. Intestinal Primer Design and Real-Time Quantitative PCR Design

The primers used in the RT-qPCR were designed based on ten gene sequences from the Genbank database, using Real-Time Primer Design Tool software (IDT DNA, Coralville, IA, USA). The sequences and the description of the primers used in this work are found in Table 1. The *Gallus gallus* 18s rRNA primer was designed as the reference gene, and the results obtained from the qPCR system were used to normalize the primers listed in Table 1. As previously described [62,63,72,73], all real-time quantitative PCR procedures were conducted with the specific primers listed in Table 1.

Table 1. Primer sequences used in the study.

Target Gene	Forward (5'-3')	Reverse (3'-5')	Amplicon Length (Base Pairs)	NCBI Accession	Ref.
Inflammatory Genes					
NF- κ B	CACAGCTGGAGGGAAGTAAAT	TTGAGTAAGGAAGTGAGGTTGAG	100	2130627	
TNF- α	GACAGCCTATGCCAACAAAGTA	TTACAGGAAGGGCAACTCATC	109	53854909	
IL-1 β	TCATCCATCCCAAGTTCATTC	GACACACTTCTCTGCCATCTT	105	395872	
IL-6	ACCTCATCTCCGAGACTTTA	GCACTGAAACTCTGGTCTT	105	302315692	
Brush Border Membrane (BBM) Functionality Genes					
OCN	GTCTGTGGGTTCTCATCGT	GTTCTTACCCACTCTCCA	124	396026	[74]
MUC2	CCTGCTGCAAGGAAGTAGAA	GGAAGATCAGAGTGGTGCATAG	272	423101	
AP	CGTCAGCCAGTTTACTATGTA	CTCTCAAAGAAGCTGAGGATGG	138	45382360	
SI	CCAGCAATGCCAGCATATG	CGGTTTCTCTTACCCTTCTT	95	2246388	
SGLT1	GCATCCTTACTCTGTGGTACTG	TATCCGCACATCACACATCC	106	8346783	
18S rRNA	GCAAGACGAACTAAAGCGAAAG	TCGGAACACGACGGTATCT	100	7262899	

NF- κ B, nuclear factor kappa-light-chain-enhancer of activated B cells; TNF- α , tumor necrosis factor-alpha; IL-1 β : interleukin one beta; IL-6: interleukin 6; OCN: occludin; MUC2, mucin 2; AP: aminopeptidase; SI: sucrose isomaltase; SGLT1: sodium-glucose transporter 1; 18S rRNA: 18S ribosomal subunit. Target genes were created from accessions within National Center for Biotechnology Information (NCBI).

2.8. Intestinal Content DNA Isolation, Bacterial Primer Design, and PCR Amplification of Bacterial 16S rDNA

Frozen cecal contents were placed into a sterile tube containing 9 mL of phosphate-buffered saline (PBS) (Catalog#75800-998, VWR, Radnor, PA, USA) and homogenized with silicone bead-beating for 3 min [67,75,76]. All procedures were conducted as previously described [63,67,72].

As previously described [76–79], primers for *Lactobacillus*, *Bifidobacterium*, *Clostridium*, *Escherichia coli*, and *Klebsiella* were used with a universal primer variable region in bacterial 16S rRNA and were used as an internal standard. The PCR products were loaded on 2% agarose gel, stained with ethidium bromide, and quantified by Quantity-One 1D analysis software version 4.6.8 (BioRad, Hercules, CA, USA). The results were given by proportions of each bacterial group compared to the universal primer, giving relative abundance as previously conducted and demonstrated, with primers listed in Table 2 [62,63,72,73,80].

Table 2. Microbial primer sequences for bacteria within cecum.

Target Gene	Forward (5'-3')	Reverse (3'-5')	Ref.
<i>Lactobacillus</i> spp.	CATCCAGTGCAAACCTAAGAG	GATCCGCTTGCCTTCGCA	[77]
<i>Bifidobacterium</i> spp.	GGGTGGTAATGCCGGATG	CCACCGTTACACCGGGAA	[77]
<i>E. coli</i> spp.	GACCTCGGTTTGTTCACAGA	CACACGCTGACGCTGACCA	[77]
<i>Clostridium</i> spp.	AAAGGAAGATTAATACCGCATAA	ATCTTGCACCGTACTCCCC	[77]
<i>Klebsiella</i> spp.	CGCGTACTATACGCCATGAACGTA	ACCGTTGATCACTTCGGTCAGG	[78,79]
16S rRNA	CGTGCCAGCCGCGTAATACG	GGGTTGCGCTCGTTGCGGGACTTAACCCAACAT	[77]

2.9. Morphological Examination

As previously described [54,65–67,81–85], intestinal samples (duodenum) were collected after the study and fixed in 4% (*v/v*) buffered formaldehyde. The samples were fixed further in 4% (*v/v*) buffered formaldehyde, dehydrated, cleared, and embedded in paraffin. The duodenum tissue was cut into 5 μ m sections and placed on positively charged slides. Sections were: deparaffinized in xylene, rehydrated in different concentrations of alcohol, and stained. Periodic acid–Schiff and Alcian blue were used to distinguish neutral (magenta) and acidic (blue) mucins. Four sections of the duodenum per chick ($n = 5$ per treatment group) were examined. Villus height, villus width, crypt depth, goblet cell number, and goblet cell diameter were measured in each segment, using light microscopy with CellSens Standard version 3.2 (Olympus Corporation, Tokyo, Japan). Villi height was measured using the lamina propria as the base; villi width, the depth of the crypt, and the number of goblet cells were counted per side of a cross-sectional view through the villus; goblet cell size was measured as the diameter of the goblet cells (μ m²). Villi surface area

was calculated from the villus height and width at half height according to Uni et al. [86] and calculated using the following equation:

$$\text{Villus surface area} = 2 \prod \times \frac{VW}{2} \times VL \quad (1)$$

where VW is the average of three measurements of villus width, and VL is the villus length [87]. For the Alcian Blue and periodic acid–Schiff stain, the segments were counted for the types of goblet cells in the villi epithelium and goblet cells within the crypts. Goblet cells were counted in ten randomly selected villi or crypts per intestinal section (four intestinal sections per subject, 40 villi or crypts counted per subject). Goblet cell type was identified based on color, as periodic acid–Schiff and Alcian blue stains distinguishes between neutral (magenta), mixed (purple), and acidic (blue) mucins. Paneth cells were identified by their triangular shape within 10 randomly selected crypts per intestinal section and then counted and measured. The means were utilized for statistical analysis.

2.10. Statistical Analysis

Experimental treatments for the in ovo assay were arranged entirely randomly. The Shapiro–Wilk test was used to assess for normality. Statistical analyses were performed using one-way Analysis of Variance (ANOVA). Data is presented as means and standard deviations. Differences were considered significant at $p < 0.05$ using a post hoc Duncan or Tukey test was used to compare different NEC severity treatments, as described in figure or table legends. Statistical analysis was conducted using SPSS version 27.0 software (IBM, Armonk, NY, USA).

3. Results

3.1. Gross Physical Findings

There was a total hatchability rate of 95%. As shown in Table 3, there was no significant difference between body weight observed between DSS treatment groups and the controls. However, the cecum weight in the DSS treatment groups (0.1% and 0.5%) was significantly higher compared to the no-injection group ($p < 0.05$, Table 2).

Table 3. The effect of DSS on the body weight, cecum weight, and cecum-to-body-weight ratio.

Group	Body Weight (g)	Cecum Weight (g)	Cecum: Body Weight
No Injection	40.06 ± 4.06 ^b	0.42 ± 0.06 ^b	0.015 ± 0.005 ^a
H ₂ O Injection	47.49 ± 1.21 ^a	0.47 ± 0.03 ^{a,b}	0.010 ± 0.001 ^a
0.1% DSS	45.81 ± 1.23 ^{a,b}	0.62 ± 0.08 ^a	0.013 ± 0.002 ^a
0.25% DSS	45.25 ± 1.01 ^{a,b}	0.49 ± 0.05 ^{a,b}	0.011 ± 0.001 ^a
0.50% DSS	45.24 ± 1.11 ^{a,b}	0.64 ± 0.08 ^a	0.014 ± 0.002 ^a
0.75% DSS	45.78 ± 0.86 ^{a,b}	0.60 ± 0.06 ^{a,b}	0.010 ± 0.000 ^a

Values are means ± stand error, $n = 8–10$. ^{a,b} within a column, means without a common letter are significantly different, $p < 0.05$ (Duncan's post-hoc test).

Additionally, intra-abdominal abscesses were found within the proventriculus and gizzard within only the 0.5% and 0.75% DSS treatments (depicted in Supplementary Figure S1).

3.2. Hb Concentration and Hepatic Glycogen Levels

The Hb value in the 0.75% DSS treatment group was significantly higher than the water injected, 0.1% DSS, and 0.25% DSS treatment groups (Table 4). Furthermore, there was a significant ($p < 0.05$) difference between the 0.75% DSS group and all other hepatic glycogen treatment groups.

Table 4. Blood hemoglobin (Hb) concentrations (g/dL) and hepatic glycogen levels (mg/mL).

Group	Hb (g/dL)	Hepatic Glycogen (mg/mL)
No Injection	10.48 ± 1.31 ^a	0.002 ± 0.001 ^b
H ₂ O Injection	9.82 ± 0.77 ^a	0.003 ± 0.001 ^b
0.1% DSS	10.70 ± 1.16 ^a	0.003 ± 0.001 ^b
0.25% DSS	10.22 ± 1.56 ^a	0.004 ± 0.001 ^b
0.50% DSS	10.13 ± 0.77 ^a	0.004 ± 0.001 ^b
0.75% DSS	10.94 ± 3.24 ^a	0.008 ± 0.002 ^a

Values are means ± standard error, $n = 5$. ^{a,b} within a column, means without a common letter are significantly different, $p < 0.05$ (Tukey's post-hoc test).

3.3. Change of Intestinal Permeability across the Groups

DSS treatments were not significantly different from the non-treated FITC-dextran birds. However, the 0.75% DSS treatment group was significantly ($p < 0.05$, Figure 1) different than the other treatment groups treated with FITC-dextran. Furthermore, no dose-response occurred from the titration of concentrations between the experimental groups and controls.

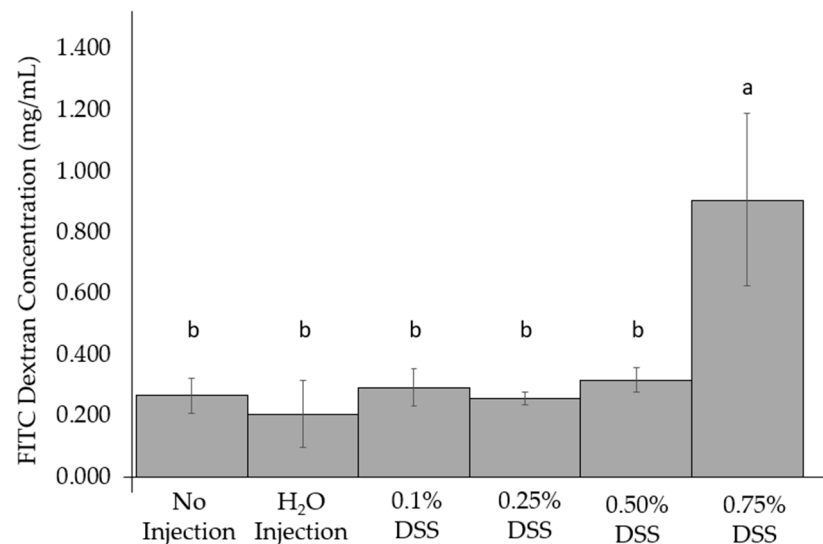


Figure 1. Comparison of the intra-amniotic administration of DSS to controls on the day of hatch within the small intestine (duodenum). Values are means ± stand error, $n = 3$. ^{a,b} within a column, means without a common letter are significantly different, $p < 0.05$ (Duncan's post-hoc test).

3.4. Duodenal Gene Expression

The gene expression of the inflammatory marker, NF- κ B1, was lower ($p < 0.05$) in the 0.50% and 0.75% DSS treatment groups compared to the control groups (no injection and H₂O injection) (Figure 2). However, other concentrations of DSS did not affect the expression of NF- κ B1 ($p < 0.05$). The relative expression of TNF- α was significantly ($p < 0.05$) decreased in all of the DSS experimental groups (0.1%, 0.25%, 0.5%, and 0.75%) compared to the controls. Similarly, IL-6 was lowered in all of the DSS-treated groups compared only to the H₂O injection group (Figure 2). However, no significant differences in IL-1 β expression were found between any of the groups.

	NF-κB	TNF-α	IL-1β	IL-6	OCLN	MUC2	AP	SI	SGLT1
No Injection	11.685 ± 0.637 ^{ab}	3.158 ± 0.187 ^b	1.017 ± 0.002 ^a	1.197 × 10 ⁵ ± 4.176 × 10 ⁴ ^a	1.094 ± 0.003 ^a	11.697 ± 1.230 ^b	1.493 ± 0.022 ^b	2.632 ± 0.018 ^a	0.94 ± 0.003 ^{ab}
H ₂ O Injection	13.651 ± 1.050 ^a	3.477 ± 0.066 ^a	1.015 ± 0.005 ^a	3.535 × 10 ⁵ ± 1.188 × 10 ⁵ ^a	1.100 ± 0.007 ^a	14.521 ± 0.775 ^a	1.536 ± 0.016 ^a	2.623 ± 0.020 ^a	0.927 ± 0.008 ^b
0.1% DSS	10.899 ± 1.076 ^{bc}	2.846 ± 0.158 ^c	1.023 ± 0.005 ^a	5.959 × 10 ⁴ ± 3.694 × 10 ⁴ ^b	1.096 ± 0.003 ^b	9.75 ± 1.076 ^{bc}	1.46 ± 0.015 ^{bc}	2.673 ± 0.022 ^a	0.94 ± 0.007 ^{ab}
0.25% DSS	10.065 ± 0.278 ^c	2.692 ± 0.019 ^c	1.02 ± 0.003 ^a	2.654 × 10 ⁴ ± 2.771 × 10 ³ ^b	1.091 ± 0.003 ^b	8.92 ± 0.160 ^c	1.432 ± 0.004 ^c	2.648 ± 0.023 ^a	0.944 ± 0.003 ^a
0.50% DSS	9.463 ± 0.198 ^c	2.65 ± 0.026 ^c	1.023 ± 0.001 ^a	2.796 × 10 ⁴ ± 4.731 × 10 ³ ^b	1.091 ± 0.001 ^b	8.707 ± 0.187 ^c	1.431 ± 0.005 ^c	2.678 ± 0.025 ^a	0.948 ± 0.002 ^a
0.75% DSS	9.014 ± 0.222 ^c	2.582 ± 0.033 ^c	1.026 ± 0.000 ^a	2.048 × 10 ⁴ ± 2.427 × 10 ³ ^b	1.092 ± 0.001 ^b	8.319 ± 0.178 ^c	1.425 ± 0.004 ^c	2.650 ± 0.020 ^a	0.951 ± 0.002 ^a


Low AU  High AU

Figure 2. Effect of the intra-amniotic administration of DSS on intestinal gene expression on the day of hatch within the small intestine (duodenum). Values are means ± stand error, $n = 5$. ^{a,b,c} within a column, means without a common letter are significantly different, $p < 0.05$ (Duncan’s post-hoc test). NF-κβ, nuclear factor kappa-light-chain-enhancer of activated B cells; TNF-α, tumor necrosis factor-alpha; IL-1β: interleukin one beta; IL-6: interleukin 6; OCLN: occludin; MUC2, mucin 2; AP: aminopeptidase; SI: sucrose isomaltase; SGLT1: sodium-glucose transporter 1; 18s rRNA: 18S ribosomal subunit.

The gene expression of brush border membrane functionality proteins, sucrose isomaltase (SI), and occludin (OCLN) were not significantly different. Despite no significant difference in OCLN gene expression, there was a trend of decreased gene expression with increased DSS treatment concentration (Figure 2). There was a significant ($p < 0.05$) down-regulation of MUC2 and AP gene expression in the DSS treatment groups compared to the H₂O and no-injection control. There is a significant increase ($p < 0.05$) in the gene expression of SGLT1 in the 0.25%, 0.50%, and 0.75% DSS-treatment groups compared to the H₂O-injected group.

3.5. Microbial Dysbiosis

Figure 3 shows cecal bacterial populations. The relative abundance of *Bifidobacterium* spp. was significantly decreased in the DSS-treated groups ($p < 0.05$) relative to the control groups (non-injected and H₂O-injected groups). *Bifidobacterium* spp. and *Lactobacillus* spp. were significantly decreased in the 0.50% and 0.75% DSS groups compared to the non-injected and H₂O-injected groups. The highest relative abundances of *Lactobacillus* spp. were in 0.1% and 0.25% DSS following the exposure compared to the controls.

	<i>Bifidobacterium</i>	<i>Lactobacillus</i>	<i>E. coli</i>	<i>Clostridium</i>	<i>Klebsiella</i>
No Injection	0.873 ± 0.004 ^a	0.754 ± 0.014 ^{bc}	0.901 ± 0.009 ^b	1.197 ± 0.012 ^a	1.081 ± 0.054 ^b
H ₂ O Injection	0.839 ± 0.01 ^b	0.773 ± 0.015 ^b	0.885 ± 0.011 ^{bc}	1.23 ± 0.010 ^a	1.142 ± 0.057 ^b
0.1% DSS	0.789 ± 0.011 ^c	0.823 ± 0.015 ^a	0.843 ± 0.036 ^c	1.196 ± 0.022 ^a	1.124 ± 0.032 ^b
0.25% DSS	0.739 ± 0.007 ^d	0.838 ± 0.007 ^a	0.908 ± 0.005 ^b	1.072 ± 0.014 ^b	1.136 ± 0.026 ^b
0.50% DSS	0.753 ± 0.004 ^d	0.725 ± 0.007 ^c	1.013 ± 0.008 ^a	1.077 ± 0.008 ^b	1.386 ± 0.018 ^a
0.75% DSS	0.727 ± 0.017 ^d	0.689 ± 0.010 ^d	1.029 ± 0.013 ^a	1.104 ± 0.024 ^b	1.472 ± 0.033 ^a


Low AU  High AU

Figure 3. Effect of the intra-amniotic administration of DSS on cecal bacterial populations (day of hatch). Values are means ± SEM. Per bacterial category, ^{a-d} within a column, treatment groups that do not share letters are significantly different according to one-way ANOVA with Tukey’s post-hoc test ($p < 0.05$).

E. coli and *Klebsiella* spp., opportunistic and possibly pathogenic bacteria, were significantly increased ($p < 0.05$) in the two highest concentrations of DSS (0.50% and 0.75%) compared with the non-injected and the H₂O-injected groups. However, the relative abun-

dance of *Clostridium* spp. was significantly ($p < 0.05$) lowered in 0.25%, 0.50%, and 0.75% DSS compared to the control groups (non-injected and H₂O-injected groups) and 0.1% DSS group.

3.6. Intestinal Morphology

The villus surface area and crypt goblet cell diameter were significantly ($p < 0.05$) lowered in the 0.75% DSS group compared to the H₂O injection group (Table 5, images withing Supplemental Figure S2), indicating that DSS negatively impacted intestinal development. A significant ($p < 0.05$, Table 5) increase was found in the villi goblet cell diameters, Paneth cell number, and Paneth cell diameter of 0.1% and 0.75% DSS groups compared to the non-injected and H₂O-injected groups. There was no significant difference in crypt depth between experimental groups.

Table 5. Effects on intestinal villi and crypts of the duodenum after the intra-amniotic administration of experimental DSS.

Treatment	Villus Surface Area (μm^2)	Crypt Depth (μm)	Villi Goblet Diameter (μm)	Crypt Goblet Diameter (μm)	Paneth Cell #	Paneth Cell Diameter (μM)
No Injection	109.99 \pm 3.06 ^d	25.17 \pm 0.93 ^{a,b}	3.57 \pm 0.05 ^d	2.99 \pm 0.05 ^b	1.09 \pm 0.02 ^c	1.56 \pm 0.03 ^b
H ₂ O Injection	205.15 \pm 5.03 ^a	26.35 \pm 0.98 ^{a,b}	4.04 \pm 0.06 ^c	3.16 \pm 0.04 ^a	1.03 \pm 0.01 ^c	1.47 \pm 0.02 ^c
0.1% DSS	147.51 \pm 3.28 ^b	27.89 \pm 1.08 ^a	4.55 \pm 0.07 ^a	2.99 \pm 0.04 ^b	1.80 \pm 0.05 ^b	1.69 \pm 0.03 ^a
0.75% DSS	130.35 \pm 0.03 ^c	24.32 \pm 0.78 ^b	4.25 \pm 0.05 ^b	2.73 \pm 0.04 ^c	1.93 \pm 0.06 ^a	1.67 \pm 0.03 ^a

Values are means \pm stand error, $n = 5$. ^{a-d} within a column means without a common letter are significantly different, $p < 0.05$ (Duncan's post-hoc test). # Number of cells.

A closer investigation of goblet cells within crypts and villi was viewed to determine differences (Table 6). Crypt goblet cell count was significantly increased in the 0.1% and 0.75% DSS groups compared to the non-injected and H₂O injection groups. Different goblet cell types were analyzed in crypts; acidic goblet cells were significantly higher ($p < 0.05$) in the 0.1% and 0.75% DSS groups compared to the control groups. There was a significantly ($p < 0.05$) higher amount of mixed goblet cells in crypts within the 0.1% DSS group compared to the control groups. Similarly, the villi goblet cell number and the acidic and mixed goblet cell number were significantly increased with 0.1% DSS exposure compared with the controls, as seen in Table 6.

Table 6. Effects on intestinal villi and crypt goblet cells of the duodenum after the intra-amniotic administration of experimental DSS.

Treatment	Crypt Goblet Cell #	Crypt Goblet Cell Type Number			Villi Goblet Cell #	Villi Goblet Cell Type Number		
		Acidic	Neutral	Mixed		Acidic	Neutral	Mixed
No Injection	8.57 \pm 0.32 ^c	6.59 \pm 0.26 ^c	0.00 \pm 0.0	1.97 \pm 0.18 ^d	15.78 \pm 0.45 ^c	13.7 \pm 0.42 ^c	0.00 \pm 0.00	2.08 \pm 0.13 ^c
H ₂ O Injection	7.96 \pm 0.24 ^c	7.42 \pm 0.22 ^b	0.00 \pm 0.00	0.49 \pm 0.06 ^c	22.93 \pm 0.6 ^b	18.4 \pm 0.53 ^b	0.00 \pm 0.00	4.53 \pm 0.23 ^b
0.1% DSS	14.7 \pm 0.41 ^a	10.23 \pm 0.31 ^a	0.00 \pm 0.00	4.47 \pm 0.19 ^a	30.37 \pm 0.84 ^a	23.91 \pm 0.68 ^a	0.00 \pm 0.00	6.46 \pm 0.36 ^a
0.75% DSS	13.48 \pm 0.04 ^b	9.76 \pm 0.32 ^a	0.00 \pm 0.00	3.74 \pm 0.19 ^b	16.64 \pm 0.56 ^c	14.63 \pm 0.49 ^c	0.00 \pm 0.00	2.09 \pm 0.14 ^c

Values are means \pm stand error, $n = 5$. ^{a-d} within a column means without a common letter are significantly different, $p < 0.05$ (Duncan's post-hoc test). # Number of cells.

4. Discussion

NEC is an acute inflammatory disease that results in the intestinal necrosis of the bowels, systemic sepsis, and multiorgan failure from a complex combination of pathological events, including patchy inflammation of the small intestine and intestinal hypoxic/reperfusion injuries and bacterial dysbiosis [3,13,16,88]. In our present study, we investigated the effects of dextran sodium sulfate (DSS) utilizing the *Gallus gallus* intra-amniotic administration model to mimic necrotizing enterocolitis (NEC). The present study indicates that the intra-amniotic administration of DSS at the highest concentration (0.75%) had similar findings as NEC manifestations in humans, including but not limited to the

inflammation of the small intestines, intra-abdominal abscesses of the gizzard, increased hemoglobin levels, increased permeability within the intestines, and the increased presence of potentially pathogenic bacteria. NEC has previously been induced and investigated in the rodent and pig models through hypoxic/hypothermic and/or surgical interventions to simulate the multifactorial nature of NEC in humans [6,19–21].

Current NEC in vivo models, such as rodents, pigs, and quails, have distinct strengths and weaknesses. Rodents (mice and rats) are induced to have NEC by cesarian section delivery before term, then gavage fed with the formula [19,89,90]. Mice have antibodies, and specific genetic techniques can be utilized to understand NEC pathophysiology mechanisms, whereas rats lack antibodies but are more resilient to stress [24]. Unfortunately, studies using the mouse model have shown inconsistent results, wherein data reproducibility presents potential issues [19,25–27]. While pigs have closer resemblance relative to rodents in physiology, there are drawbacks in which NEC is induced via intestinal injury to the whole intestine, and genetic techniques also present limitations. In another model, gnotobiotic quails, NEC is induced via the oral gavage of bacteria associated with NEC to affect its small intestine, which has aided in understanding the inducible nitric oxide synthase (iNOS) pathway before macroscopic lesions [34,35,91]. Quails have been shown to be an NEC model that balances practicality, resilience, and molecular manipulation [34–37]. Given these aforementioned factors and that the chicken model has been a leading system investigating vertebrate development using functional genomics and biochemistry to study diseases similar to NEC [38], we sought to develop another potential model for NEC using the embryonic stage of the *Gallus gallus*.

In our experimental trials, the intra-amniotic administration of DSS was utilized to induce intestinal inflammation to cause NEC physiopathology [92–94]. DSS is a sulfated polysaccharide with various molecular weights (5–1400 kDa), commonly used to induce enteric colitis in rodents by penetrating the intestinal mucosal membrane [19,93–96]. DSS-induced colitis is a widely used model because it is rapid, simple, reproducible, and controllable. Recent studies have shown that DSS added to DI H₂O induces clinical, gross, and histological factors associated with enteritis in broiler chickens, such as decreased body weight, bloody diarrhea, intestinal lesions, shortened villi height, and increased goblet cell density [92,94,97,98]. Furthermore, Zou et al. (2018) demonstrated that DSS exposure to broiler chickens increases gut leakiness and induces pro- and anti-inflammatory cytokine response elements in a dose-dependent manner [92]. Nevertheless, there is limited research characterizing DSS-induced NEC in *Gallus gallus*, and this study demonstrates the first-ever intra-amniotic administration of DSS to induce NEC.

During the initial necropsies, there was little to no inflammation within the internal organs of the chicks on the day of hatch in the 0.1, 0.25, and 0.5% DSS exposed groups. However, the 0.75% DSS treatment group had a few slightly patchy inflammation sites in the small intestines and showed intra-abdominal abscesses within the proventriculus and gizzard (Supplemental Figure S1); these observations are in agreement with previous studies that demonstrated the initial hypoxic and reperfusion injuries (typical in NEC cases from rodents and clinical models) and an increase in innate immune responses (cytokines and white blood cells). [11,20,24,92,99]. The intra-abdominal abscesses and patchy inflammation in the distal digestive organs resulting from the treatment with the highest DSS concentration (0.75%) can be associated with hypoxic reperfusion injuries, which have previously been demonstrated with DSS exposure [92,94,95]. To further illustrate the effectiveness of DSS penetrating through the mucosal layers of the small intestine, a FITC-dextran assay was performed (Figure 1). Compared to all other groupings, there was a significant ($p < 0.05$) increase in the intestinal mucosal layer penetration in the 0.75% DSS treatment group. The increased intestinal permeability suggests that the DSS successfully breaks down the mucosal layer, potentially allowing pathogenic bacteria to invade the host's villi, as previously described [9,25,69,100,101]. However, occludin (OCLN) gene expression, a tight junction protein between the intestinal enterocytes, does not significantly differ between the groups (Figure 2). The lack of significance of the gene expression of the

tight junctions on the basolateral surface could be the short duration of a DSS exposure time to allow for occludin degradation. Though no significant alterations in OCLN gene expression were found, our results supporting increased intestinal permeability with DSS exposure were further supported by our hemoglobin and hepatic glycogen results. The hemoglobin concentration was raised within the DSS groups compared to the non-injected group (Table 4). As intestinal irritability and instability increase, hemoglobin values were found to increase in clinical patients with inflammatory bowel disease [102]. Hepatic glycogen levels were increased only within the 0.75% DSS group compared to others (Table 4). However, Sodhi et al. (2009) demonstrated that enterocyte proliferation is inhibited in rat intestinal cell lines (IEC-6 cells enterocytes) and TLR4^{-/-} mice and that glycogen synthase kinase decreases when under NEC conditions with lipopolysaccharides [103]. This observed difference could be due to the treatment to induce the condition and the difference between the models utilized.

Brush border membrane (BBM) functionality was investigated by measuring the gene expression of the functional proteins viewing the digestive capabilities, as seen in Figure 2. There was no significant difference between the treatment groups in sucrose isomaltase or sodium–glucose transporter 1. However, there was a substantial lowering of mucin 2 (MUC2) and aminopeptidase (AP) gene expression in the DSS treatment groups (0.25%, 0.50%, and 0.75%) compared to the no-injection and H₂O-injection groups. As previously mentioned, DSS is a sulfated polysaccharide that disrupts the luminal mucus layer, allowing mucosal thinning and opportunistic bacteria to penetrate the BBM, causing intestinal trauma [104,105]. This reasoning on MUC2 supports the findings on the lowering of aminopeptidase expression, as AP is primarily located near the apical side of the lumen in the intestinal epithelial cells [106]. Aminopeptidases are enzymes that catalyze the amino terminus of a protein within subcellular organelles, cytosol, and membrane components. Thus, it can be suggested that, if the BBM membrane is injured, the AP capacity would be significantly reduced, increasing the possibility of immune responses (pro-inflammation and apoptosis) [107].

Inflammation resulting from NEC is a primary identifier of injury from hypoxia/reperfusion conditions and an indicative marker for the disease [15,32,108,109]. Inflammation biomarkers, nuclear factor kappa-light-chain-enhancer of activated B cells (NF- κ B), tumor necrosis factor-alpha (TNF- α), interleukin one beta (IL-1 β), and interleukin 6 (IL-6) were all analyzed via RT-qPCR (Figure 2) due to the use of these biomarkers in other NEC models and clinical trials [108–112]. NF- κ B and TNF- α were significantly ($p > 0.05$) lower in the 0.50% and 0.75% DSS groups compared to the control groups (non-injected and H₂O-injected). The downregulation of NF- κ B gene expression originates from the upstream signaling of TNF- α being downregulated since these proteins operate in tandem with pro-inflammation pathways triggered by microbial products (i.e., endotoxins, metabolites, amino acids, etc.) and signal transductions mechanisms in the innate immune system [113–117]. The downregulation of TNF- α is potentially derived from the upregulation of microbial byproducts within the duodenum in the DSS treatments. Krishnaveni and Jayachandran (2009) found that ethyl acetate extracts from two different marine bacteria caused the downregulation of TNF- α [118]. Similarly, Lou et al. (2018) found that *Brucella* caused the same downregulation of TNF- α within porcine and murine models [119].

There were significant changes within the bacterial profiles in the DSS treatment groups (Figure 3). Bacterial profiles of the 0.75% DSS group were significantly ($p < 0.05$) lower abundance of *Bifidobacterium*, *Lactobacillus*, and *Clostridium* spp. In contrast, the DSS-treatment groups demonstrated significantly higher abundance levels of *E. coli* and *Klebsiella* spp. ($p < 0.05$). The lower abundance of beneficial bacteria (*Bifidobacterium* and *Lactobacillus*) suggests an opportunity for dysbiosis via the proliferation of opportunistic bacteria such as *E. coli* and *Klebsiella*. Our results are similar to other NEC models that utilized different treatments to induce NEC [6,9,17,20,24,26,34,91,120]. One of the first NEC models used *Klebsiella* to create an NEC model (mice) because the genus produces hydrogen-sulfide-rich gas pockets of pneumatosis in vivo [22,121]. Similarly, it is theorized that gas produced by *E. coli* can invade the same intraluminal cavities as *Klebsiella*, which leads

to pneumatosis intestinalis, which is a radiographic sign of NEC [122–125]. Additionally, Tarracchini et al. (2021) found that *E. coli* and other opportunistic bacteria are found within the next-generation sequencing of NEC clinical patients, suggesting that the bacterial abundance of *E. coli* could induce NEC pathology [126]. These invasive bacterial changes the grouping/profile of the gut and influences the intestinal BBM morphology [126–132].

Within this study, the duodenum was sectioned to investigate DSS's effect on its intestinal morphology (Supplemental Figure S2). Previous studies have shown that NEC results in various levels of intestinal degradation due to microbial dysbiosis effects on the brush border membrane morphology (i.e., the villi surface area, goblet cell number, type, size, Paneth cell production) [133–135]. The 0.75% DSS treatment group had significantly lower villus surface area, crypt goblet cell diameter, and villi goblet cell number and type. In parallel, there was a significant increase in the Paneth cell number and size (Table 5) and crypt goblet cell number and types (Table 6) populations. Since goblet cells produce mucin, which lubricates the passage of food through the intestines and protects the intestine from the potential damage from digestive enzymes, the DSS treatments at the highest concentration would be associated with damage at the apical side of the enterocyte while lowering the villus surface area, which aligns with previous DSS studies and is in agreement with the present study [136–138]. Additionally, on the enterocyte's basolateral side, the crypts' goblet cells would anticipate the loss of mucin and increase its mucin production to overcome the loss [139,140]. This anticipation can be further supported by the increase in Paneth cell findings within the crypts of the intestinal epithelial cells ($p < 0.05$, Table 5). Paneth cells within the small intestine synthesize and secrete antimicrobial enzymes as a part of the innate immune system [100,141,142]. The antimicrobial peptide secretion by Paneth cells is recognized by MyD88-dependent Toll-like receptor (TLR) activations, triggering the expression of multiple peptides and proteins [19,25]. The Paneth cells migrate towards the base of the villi after differentiation within the crypts to protect commensal bacteria from the opportunistic bacteria within the gut, which supports the findings of bacterial dysbiosis mentioned earlier in Figure 3.

5. Conclusions

This study is the first to demonstrate NEC symptoms via the intra-amniotic administration of DSS in vivo (*Gallus gallus*). The 0.75% DSS treatment group decreased BBM functionality and demonstrated microbiota dysbiosis within a premature gut, mimicking other models of NEC. Although we did not observe significant severe pathologies (gas-filled lesions or necrotic plaques in histological sectioning), there was a clear trend of opportunistic bacterial populations proliferation and overtaking the distal gastrointestinal tract. This transformation of untreated and DSS-treated individuals' microbial profiles can potentially affect several bacterial metabolic pathways related to bacterial, cellular, and metabolic processes. The results of this study are promising evidence to investigate increased concentrations of DSS to cause more severe NEC symptoms and identify potential novel biomarkers for less severe NEC cases. Furthermore, the suggested in vivo novel model and innovative approach will support the assessment of various potential interventions to ameliorate the pathophysiology of NEC.

Supplementary Materials: The following are available online at <https://www.mdpi.com/article/10.3390/nu14224795/s1>, Figure S1: Representative images of gross anatomical photos of dissections and proventriculus/gizzards of birds on the day of hatch; Figure S2: Representative histology (Alcian Blue and Pacific Acid Schiff staining) images of the duodenum of birds on the day of hatch.

Author Contributions: N.K. and E.T. conceived and designed the experiment. N.K., J.C. and C.D.J. collected and analyzed the data and wrote the initial draft. N.K., J.C., C.D.J. and E.T. reviewed and edited the manuscript. E.T. led the research. All authors have read and agreed to the published version of the manuscript.

Funding: This research received no external funding.

Institutional Review Board Statement: The animal protocol used in this study was conducted according to the guidelines of the Declaration of Helsinki and approved by the Cornell University Institutional Animal Care and Use Committee by ethic approval code 2020-0077.

Informed Consent Statement: Not applicable.

Conflicts of Interest: The authors declare no conflict of interest.

References

1. Alsaied, A.; Islam, N.; Thalib, L. Global Incidence of Necrotizing Enterocolitis: A Systematic Review and Meta-Analysis. *BMC Pediatr.* **2020**, *20*, 344. [\[CrossRef\]](#)
2. Kosloske, A. Epidemiology of Necrotizing Enterocolitis. *Acta Paediatr.* **1994**, *83*, 2–7. [\[CrossRef\]](#) [\[PubMed\]](#)
3. Eaton, S.; Rees, C.M.; Hall, N.J. Current Research on the Epidemiology, Pathogenesis, and Management of Necrotizing Enterocolitis. *Neonatology* **2017**, *111*, 423–430. [\[CrossRef\]](#) [\[PubMed\]](#)
4. Faraday, C.; Hamad, S.; Jones, K.D.; Sim, K.; Cherian, S.; James, A.; Godambe, S.; New, H.V.; Kroll, J.S.; Clarke, P. Characteristics and Incidence of Transfusion-Associated Necrotizing Enterocolitis in the UK. *J. Matern. Fetal. Neonatal. Med.* **2020**, *33*, 398–403. [\[CrossRef\]](#) [\[PubMed\]](#)
5. Chauhan, N.; Tiwari, S.; Jain, U. Potential Biomarkers for Effective Screening of Neonatal Sepsis Infections: An Overview. *Microb. Pathog.* **2017**, *107*, 234–242. [\[CrossRef\]](#)
6. Doğan, G.; İpek, H. The Development of Necrotizing Enterocolitis Publications: A Holistic Evolution of Global Literature with Bibliometric Analysis. *Eur. J. Pediatr. Surg.* **2020**, *30*, 293–303. [\[CrossRef\]](#) [\[PubMed\]](#)
7. Battersby, C.; Santhalingam, T.; Costeloe, K.; Modi, N. Incidence of Neonatal Necrotising Enterocolitis in High-Income Countries: A Systematic Review. *Arch. Dis. Child. Fetal. Neonatal Ed.* **2018**, *103*, F182–F189. [\[CrossRef\]](#) [\[PubMed\]](#)
8. De Plaen, I.G. Inflammatory Signaling in Necrotizing Enterocolitis. *Clin. Perinatol.* **2013**, *40*, 109–124. [\[CrossRef\]](#)
9. Zhang, C.; Sherman, M.P.; Prince, L.S.; Bader, D.; Weitkamp, J.-H.; Slaughter, J.C.; McElroy, S.J. Paneth Cell Ablation in the Presence of Klebsiella Pneumoniae Induces Necrotizing Enterocolitis (NEC)-like Injury in Immature Murine Small Intestine. *Dis. Model. Mech.* **2012**, *5*, 522–532. [\[CrossRef\]](#)
10. Bazacliu, C.; Neu, J. Pathophysiology of Necrotizing Enterocolitis: An Update. *Curr. Pediatr. Rev.* **2019**, *15*, 68–87. [\[CrossRef\]](#)
11. Meister, A.L.; Doheny, K.K.; Travagli, R.A. Necrotizing Enterocolitis: It's Not All in the Gut. *Exp. Biol. Med.* **2020**, *245*, 85–95. [\[CrossRef\]](#) [\[PubMed\]](#)
12. Rich, B.S.; Dolgin, S.E. Necrotizing Enterocolitis. *Pediatr. Rev.* **2017**, *38*, 552–559. [\[CrossRef\]](#) [\[PubMed\]](#)
13. Müller, M.J.; Paul, T.; Seeliger, S. Necrotizing Enterocolitis in Premature Infants and Newborns. *NPM* **2016**, *9*, 233–242. [\[CrossRef\]](#)
14. Adams-Chapman, I. Necrotizing Enterocolitis and Neurodevelopmental Outcome. *Clin. Perinatol.* **2018**, *45*, 453–466. [\[CrossRef\]](#)
15. Molteni, M.; Gemma, S.; Rossetti, C. The Role of Toll-Like Receptor 4 in Infectious and Noninfectious Inflammation. *Mediat. Inflamm.* **2016**, *2016*, 6978936. [\[CrossRef\]](#)
16. Tirone, C.; Pezza, L.; Paladini, A.; Tana, M.; Aurilia, C.; Lio, A.; D'Ippolito, S.; Tersigni, C.; Posteraro, B.; Sanguinetti, M.; et al. Gut and Lung Microbiota in Preterm Infants: Immunological Modulation and Implication in Neonatal Outcomes. *Front. Immunol.* **2019**, *10*, 2910. [\[CrossRef\]](#)
17. Schnabl, K.-L.; Van Aerde, J.-E.; Thomson, A.-B.; Clandinin, M.-T. Necrotizing Enterocolitis: A Multifactorial Disease with No Cure. *World J. Gastroenterol.* **2008**, *14*, 2142–2161. [\[CrossRef\]](#) [\[PubMed\]](#)
18. Alganabi, M.; Lee, C.; Bindi, E.; Li, B.; Pierro, A. Recent Advances in Understanding Necrotizing Enterocolitis. *F1000Research* **2019**, *8*, 107. [\[CrossRef\]](#) [\[PubMed\]](#)
19. Jilling, T.; Simon, D.; Lu, J.; Meng, F.J.; Li, D.; Schy, R.; Thomson, R.B.; Soliman, A.; Ardit, M.; Caplan, M.S. The Roles of Bacteria and TLR4 in Rat and Murine Models of Necrotizing Enterocolitis. *J. Immunol.* **2006**, *177*, 3273–3282. [\[CrossRef\]](#)
20. Di Lorenzo, M.; Bass, J.; Krantis, A. An Intraluminal Model of Necrotizing Enterocolitis in the Developing Neonatal Piglet. *J. Pediatr. Surg.* **1995**, *30*, 1138–1142. [\[CrossRef\]](#)
21. Kappel, S.S.; Sangild, P.T.; Hilsted, L.; Hartmann, B.; Thymann, T.; Aunsholt, L. Gastric Residual to Predict Necrotizing Enterocolitis in Preterm Piglets As Models for Infants. *J. Parenter. Enter. Nutr.* **2021**, *45*, 87–93. [\[CrossRef\]](#) [\[PubMed\]](#)
22. Barlow, B.; Santulli, T.V.; Heird, W.C.; Pitt, J.; Blanc, W.A.; Schullinger, J.N. An Experimental Study of Acute Neonatal Enterocolitis—The Importance of Breast Milk. *J. Pediatr. Surg.* **1974**, *9*, 587–595. [\[CrossRef\]](#)
23. Sodhi, C.; Richardson, W.; Gribar, S.; Hackam, D.J. The Development of Animal Models for the Study of Necrotizing Enterocolitis. *Dis. Model. Mech.* **2008**, *1*, 94–98. [\[CrossRef\]](#)
24. Sulisty, A.; Rahman, A.; Biouss, G.; Antounians, L.; Zani, A. Animal Models of Necrotizing Enterocolitis: Review of the Literature and State of the Art. *Innov. Surg. Sci.* **2018**, *3*, 87–92. [\[CrossRef\]](#) [\[PubMed\]](#)
25. White, J.R.; Gong, H.; Pope, B.; Schlievert, P.; McElroy, S.J. Paneth Cell Disruption-Induced Necrotizing Enterocolitis Requires Live Bacteria and Occurs Independent of TLR4 Signaling. *Dis. Model. Mech.* **2017**, *10*, 727–736. [\[CrossRef\]](#)
26. Lyu, C.; Jiang, S.; Kong, M.; Chen, X.; Zhang, L. Vitamin D Protects against Necrotising Enterocolitis in Newborn Mice by Activating the ERK Signalling Pathway. *Mol. Med. Rep.* **2020**, *22*, 2107–2114. [\[CrossRef\]](#)

27. MohanKumar, K.; Kaza, N.; Jagadeeswaran, R.; Garzon, S.A.; Bansal, A.; Kurundkar, A.R.; Namachivayam, K.; Remon, J.I.; Bandepalli, C.R.; Feng, X.; et al. Gut Mucosal Injury in Neonates Is Marked by Macrophage Infiltration in Contrast to Pleomorphic Infiltrates in Adult: Evidence from an Animal Model. *Am. J. Physiol. Gastrointest. Liver Physiol.* **2012**, *303*, G93–G102. [[CrossRef](#)]
28. Roura, E.; Koopmans, S.-J.; Lallès, J.-P.; Le Huerou-Luron, I.; de Jager, N.; Schuurman, T.; Val-Laillet, D. Critical Review Evaluating the Pig as a Model for Human Nutritional Physiology. *Nutr. Res. Rev.* **2016**, *29*, 60–90. [[CrossRef](#)]
29. Lunney, J.K.; Van Goor, A.; Walker, K.E.; Hailstock, T.; Franklin, J.; Dai, C. Importance of the Pig as a Human Biomedical Model. *Sci. Transl. Med.* **2021**, *13*, eabd5758. [[CrossRef](#)]
30. Merrifield, C.A.; Lewis, M.; Claus, S.P.; Beckonert, O.P.; Dumas, M.-E.; Duncker, S.; Kochhar, S.; Rezzi, S.; Lindon, J.C.; Bailey, M.; et al. A Metabolic System-Wide Characterisation of the Pig: A Model for Human Physiology. *Mol. Biosyst.* **2011**, *7*, 2577. [[CrossRef](#)]
31. Holgersen, K.; Gao, X.; Narayanan, R.; Gaur, T.; Carey, G.; Barton, N.; Pan, X.; Muk, T.; Thymann, T.; Sangild, P.T. Supplemental Insulin-Like Growth Factor-1 and Necrotizing Enterocolitis in Preterm Pigs. *Front. Pediatr.* **2020**, *8*, 602047. [[CrossRef](#)] [[PubMed](#)]
32. Nguyen, D.N.; Thymann, T.; Goericke-Pesch, S.K.; Ren, S.; Wei, W.; Skovgaard, K.; Damborg, P.; Brunse, A.; van Gorp, C.; Kramer, B.W.; et al. Prenatal Intra-Amniotic Endotoxin Induces Fetal Gut and Lung Immune Responses and Postnatal Systemic Inflammation in Preterm Pigs. *Am. J. Pathol.* **2018**, *188*, 2629–2643. [[CrossRef](#)] [[PubMed](#)]
33. Di Lorenzo, M.; Bass, J.; Krantis, A. Use of L-Arginine in the Treatment of Experimental Necrotizing Enterocolitis. *J. Pediatr. Surg.* **1995**, *30*, 235–241. [[CrossRef](#)]
34. Waligora-Dupriet, A.J.; Dugay, A.; Auzeil, N.; Nicolis, I.; Rabot, S.; Huerre, M.R.; Butel, M.J. Short-Chain Fatty Acids and Polyamines in the Pathogenesis of Necrotizing Enterocolitis: Kinetics Aspects in Gnotobiotic Quails. *Anaerobe* **2009**, *15*, 138–144. [[CrossRef](#)] [[PubMed](#)]
35. Waligora-Dupriet, A.-J.; Dugay, A.; Auzeil, N.; Huerre, M.; Butel, M.-J. Evidence for Clostridial Implication in Necrotizing Enterocolitis through Bacterial Fermentation in a Gnotobiotic Quail Model. *Pediatr. Res.* **2005**, *58*, 629–635. [[CrossRef](#)]
36. Baer, J.; Lansford, R.; Cheng, K. Japanese Quail as a Laboratory Animal Model. In *Laboratory Animal Medicine*; Elsevier: Amsterdam, The Netherlands, 2015; pp. 1087–1108. ISBN 978-0-12-409527-4.
37. Ares, G.J.; McElroy, S.J.; Hunter, C.J. The Science and Necessity of Using Animal Models in the Study of Necrotizing Enterocolitis. *Semin. Pediatr. Surg.* **2018**, *27*, 29–33. [[CrossRef](#)]
38. Dodgson, J.B.; Romanov, M.N. Use of Chicken Models for the Analysis of Human Disease. *Curr. Protoc. Hum. Genet.* **2004**, *40*, 15.5.1–15.5.12. [[CrossRef](#)]
39. Huang, H.; Liu, L.; Li, C.; Liang, Z.; Huang, Z.; Wang, Q.; Li, S.; Zhao, Z. Fat Mass- and Obesity-Associated (FTO) Gene Promoted Myoblast Differentiation through the Focal Adhesion Pathway in Chicken. *3 Biotech* **2020**, *10*, 403. [[CrossRef](#)]
40. Cui, C.; Han, S.; Tang, S.; He, H.; Shen, X.; Zhao, J.; Chen, Y.; Wei, Y.; Wang, Y.; Zhu, Q.; et al. The Autophagy Regulatory Molecule CSRP3 Interacts with LC3 and Protects Against Muscular Dystrophy. *Int. J. Mol. Sci.* **2020**, *21*, 749. [[CrossRef](#)]
41. Sundekilde, U.K.; Rasmussen, M.K.; Young, J.F.; Bertram, H.C. High Resolution Magic Angle Spinning NMR Spectroscopy Reveals That Pectoralis Muscle Dystrophy in Chicken Is Associated with Reduced Muscle Content of Anserine and Carnosine. *Food Chem.* **2017**, *217*, 151–154. [[CrossRef](#)]
42. Thu, H.M.; Myat, T.W.; Win, M.M.; Thant, K.Z.; Rahman, S.; Umeda, K.; Nguyen, S.V.; Icatlo, F.C., Jr.; Higo-Moriguchi, K.; Taniguchi, K.; et al. Chicken Egg Yolk Antibodies (IgY) for Prophylaxis and Treatment of Rotavirus Diarrhea in Human and Animal Neonates: A Concise Review. *Korean J. Food Sci. Anim. Resour.* **2017**, *37*, 1–9. [[CrossRef](#)] [[PubMed](#)]
43. Sood, U.; Gupta, V.; Kumar, R.; Lal, S.; Fawcett, D.; Rattan, S.; Poinern, G.E.J.; Lal, R. Chicken Gut Microbiome and Human Health: Past Scenarios, Current Perspectives, and Futuristic Applications. *Indian J. Microbiol.* **2020**, *60*, 2–11. [[CrossRef](#)] [[PubMed](#)]
44. Lacharme-Lora, L.; Owen, S.V.; Blundell, R.; Canals, R.; Wenner, N.; Perez-Sepulveda, B.; Fong, W.Y.; Gilroy, R.; Wigley, P.; Hinton, J.C.D. The Use of Chicken and Insect Infection Models to Assess the Virulence of African Salmonella Typhimurium ST313. *PLoS Negl. Trop. Dis.* **2019**, *13*, e0007540. [[CrossRef](#)] [[PubMed](#)]
45. Leigh, S.A.; Branton, S.L.; Evans, J.D.; Collier, S.D. Fluorescent Microspheres as a Positive Indicator in an Intratracheal Infection Model. *J. Microbiol. Methods* **2020**, *172*, 105886. [[CrossRef](#)]
46. Ochoa-Repáraz, J.; Magori, K.; Kasper, L.H. The Chicken or the Egg Dilemma: Intestinal Dysbiosis in Multiple Sclerosis. *Ann. Transl. Med.* **2017**, *5*, 145. [[CrossRef](#)]
47. Sundick, R.S.; Bagchi, N.; Brown, T.R. The Obese Strain Chicken as a Model for Human Hashimoto’s Thyroiditis. *Exp Clin Endocrinol. Diabetes* **2009**, *104*, 4–6. [[CrossRef](#)]
48. Teixeira, A.R.L.; Nitz, N.; Bernal, F.M.; Hecht, M.M. Parasite Induced Genetically Driven Autoimmune Chagas Heart Disease in the Chicken Model. *J. Vis. Exp.* **2012**, e3716. [[CrossRef](#)]
49. Hu, J.; Ishihara, M.; Chin, A.I.; Wu, L. Establishment of Xenografts of Urological Cancers on Chicken Chorioallantoic Membrane (CAM) to Study Metastasis. *Precis. Clin. Med.* **2019**, *2*, 140–151. [[CrossRef](#)]
50. Kunz, P.; Schenker, A.; Sähr, H.; Lehner, B.; Fellenberg, J. Optimization of the Chicken Chorioallantoic Membrane Assay as Reliable in Vivo Model for the Analysis of Osteosarcoma. *PLoS ONE* **2019**, *14*, e0215312. [[CrossRef](#)]
51. Hawkrigde, A.M. The Chicken Model of Spontaneous Ovarian Cancer. *Prot. Clin. Appl.* **2014**, *8*, 689–699. [[CrossRef](#)]
52. Reed, S.; Neuman, H.; Glahn, R.P.; Koren, O.; Tako, E. Characterizing the Gut (*Gallus gallus*) Microbiota Following the Consumption of an Iron Biofortified Rwandan Cream Seeded Carioca (*Phaseolus vulgaris* L.) Bean-Based Diet. *PLoS ONE* **2017**, *12*, e0182431. [[CrossRef](#)]

53. Reed, S.; Knez, M.; Uzan, A.; Stangoulis, J.; Glahn, R.P.; Koren, O.; Tako, E. Alterations in the Gut (*Gallus gallus*) Microbiota Following the Consumption of Zinc Biofortified Wheat (*Triticum aestivum*)-Based Diet. *J. Agric. Food Chem.* **2018**, *66*, 6291–6300. [[CrossRef](#)] [[PubMed](#)]
54. Carboni, J.; Reed, S.; Kolba, N.; Eshel, A.; Koren, O.; Tako, E. Alterations in the Intestinal Morphology, Gut Microbiota, and Trace Mineral Status Following Intra-Amniotic Administration (*Gallus gallus*) of Teff (*Eragrostis Tef*) Seed Extracts. *Nutrients* **2020**, *12*, 3020. [[CrossRef](#)] [[PubMed](#)]
55. Shterzer, N.; Rothschild, N.; Sbehat, Y.; Stern, E.; Nazarov, A.; Mills, E. Large Overlap Between the Intestinal and Reproductive Tract Microbiomes of Chickens. *Front. Microbiol.* **2020**, *11*, 1508. [[CrossRef](#)] [[PubMed](#)]
56. Juste Contin Gomes, M.; Stampini Duarte Martino, H.; Tako, E. Effects of Iron and Zinc Biofortified Foods on Gut Microbiota In Vivo (*Gallus gallus*): A Systematic Review. *Nutrients* **2021**, *13*, 189. [[CrossRef](#)] [[PubMed](#)]
57. Beasley, J.T.; Johnson, A.A.T.; Kolba, N.; Bonneau, J.P.; Glahn, R.P.; Ozeri, L.; Koren, O.; Tako, E. Nicotianamine-Chelated Iron Positively Affects Iron Status, Intestinal Morphology and Microbial Populations in Vivo (*Gallus gallus*). *Sci. Rep.* **2020**, *10*, 2297. [[CrossRef](#)]
58. Reed, S.; Neuman, H.; Moscovich, S.; Glahn, R.; Koren, O.; Tako, E. Chronic Zinc Deficiency Alters Chick Gut Microbiota Composition and Function. *Nutrients* **2015**, *7*, 9768–9784. [[CrossRef](#)]
59. Tako, E.; Glahn, R.P. Iron Status of the Late Term Broiler (*Gallus gallus*) Embryo and Hatchling. *Int. J. Poult. Sci.* **2011**, *10*, 42–48. [[CrossRef](#)]
60. Warkentin, T.; Kolba, N.; Tako, E. Low Phytate Peas (*Pisum sativum* L.) Improve Iron Status, Gut Microbiome, and Brush Border Membrane Functionality In Vivo (*Gallus gallus*). *Nutrients* **2020**, *12*, 2563–2581. [[CrossRef](#)]
61. Martino, H.S.D.; Kolba, N.; Tako, E. Yacon (*Smallanthus sonchifolius*) Flour Soluble Extract Improve Intestinal Bacterial Populations, Brush Border Membrane Functionality and Morphology in Vivo (*Gallus gallus*). *Food Res. Int.* **2020**, *137*, 109705–109716. [[CrossRef](#)]
62. Dias, D.M.; Kolba, N.; Hart, J.J.; Ma, M.; Sha, S.T.; Lakshmanan, N.; Nutti, M.R.; Martino, H.S.D.; Glahn, R.P.; Tako, E. Soluble Extracts from Carioca Beans (*Phaseolus vulgaris* L.) Affect the Gut Microbiota and Iron Related Brush Border Membrane Protein Expression in Vivo (*Gallus gallus*). *Food Res. Int.* **2019**, *123*, 172–180. [[CrossRef](#)] [[PubMed](#)]
63. Wang, X.; Kolba, N.; Liang, J.; Tako, E. Alterations in Gut Microflora Populations and Brush Border Functionality Following Intra-Amniotic Administration (*Gallus gallus*) of Wheat Bran Prebiotic Extracts. *Food Funct.* **2019**, *10*, 4834–4843. [[CrossRef](#)] [[PubMed](#)]
64. Hou, T.; Tako, E. The In Ovo Feeding Administration (*Gallus gallus*)—An Emerging In Vivo Approach to Assess Bioactive Compounds with Potential Nutritional Benefits. *Nutrients* **2018**, *10*, 418–435. [[CrossRef](#)] [[PubMed](#)]
65. Agarwal, N.; Kolba, N.; Jung, Y.; Cheng, J.; Tako, E. Saffron (*Crocus sativus* L.) Flower Water Extract Disrupts the Cecal Microbiome, Brush Border Membrane Functionality, and Morphology In Vivo (*Gallus gallus*). *Nutrients* **2022**, *141*, 220–233. [[CrossRef](#)]
66. Agarwal, N.; Kolba, N.; Khen, N.; Even, C.; Turjeman, S.; Koren, O.; Tako, E. Quinoa Soluble Fiber and Quercetin Alter the Composition of the Gut Microbiome and Improve Brush Border Membrane Morphology In Vivo (*Gallus gallus*). *Nutrients* **2022**, *14*, 448–462. [[CrossRef](#)]
67. Pereira da Silva, B.; Kolba, N.; Duarte Martino, H.S.; Hart, J.J.; Tako, E. Soluble Extracts from Chia Seed (*Salvia hispanica* L.) Affect Brush Border Membrane Functionality, Morphology and Intestinal Bacterial Populations In Vivo (*Gallus gallus*). *Nutrients* **2019**, *11*, 2457–2474. [[CrossRef](#)]
68. Haahr, M.; Haahr, S. *Random Sequence Generator*; Dublin, Ireland, 2022.
69. Barekatin, R.; Chrystal, P.V.; Howarth, G.S.; McLaughlan, C.J.; Gilani, S.; Nattrass, G.S. Performance, Intestinal Permeability, and Gene Expression of Selected Tight Junction Proteins in Broiler Chickens Fed Reduced Protein Diets Supplemented with Arginine, Glutamine, and Glycine Subjected to a Leaky Gut Model. *Poult. Sci.* **2019**, *98*, 6761–6771. [[CrossRef](#)]
70. Dreiling, C.E.; Brown, D.E.; Casale, L.; Kelly, L. Muscle Glycogen: Comparison of Iodine Binding and Enzyme Digestion Assays and Application to Meat Samples. *Meat Sci.* **1987**, *20*, 167–177. [[CrossRef](#)]
71. Morais Dias, D.; Kolba, N.; Binyamin, D.; Ziv, O.; Regini Nutti, M.; Stampini Duarte Martino, H.; Glahn, R.P.; Koren, O.; Tako, E. Iron Biofortified Carioca Bean (*Phaseolus vulgaris* L.)-Based Brazilian Diet Delivers More Absorbable Iron and Affects the Gut Microbiota In Vivo (*Gallus gallus*). *Nutrients* **2018**, *10*, 1970–1990. [[CrossRef](#)]
72. Pacifici, S.; Song, J.; Zhang, C.; Wang, Q.; Glahn, R.; Kolba, N.; Tako, E. Intra Amniotic Administration of Raffinose and Stachyose Affects the Intestinal Brush Border Functionality and Alters Gut Microflora Populations. *Nutrients* **2017**, *9*, 304. [[CrossRef](#)]
73. Hou, T.; Kolba, N.; Glahn, R.; Tako, E. Intra-Amniotic Administration (*Gallus gallus*) of Cicer Arietinum and Lens Culinaris Prebiotics Extracts and Duck Egg White Peptides Affects Calcium Status and Intestinal Functionality. *Nutrients* **2017**, *9*, 785. [[CrossRef](#)] [[PubMed](#)]
74. Stephens, C.S.; Johnson, P.A. Occludin Expression and Regulation in Small Follicles of the Layer and Broiler Breeder Hen. *Gen. Comp. Endocrinol.* **2017**, *248*, 106–113. [[CrossRef](#)] [[PubMed](#)]
75. Hartono, K.; Reed, S.; Ankrah, N.A.; Glahn, R.P.; Tako, E. Alterations in Gut Microflora Populations and Brush Border Functionality Following Intra-Amniotic Daidzein Administration. *RSC Adv.* **2015**, *5*, 6407–6412. [[CrossRef](#)]
76. Tako, E.; Glahn, R.P.; Welch, R.M.; Lei, X.; Yasuda, K.; Miller, D.D. Dietary Inulin Affects the Expression of Intestinal Enterocyte Iron Transporters, Receptors and Storage Protein and Alters the Microbiota in the Pig Intestine. *Br. J. Nutr.* **2008**, *99*, 472–480. [[CrossRef](#)]

77. Zhu, X.Y.; Zhong, T.; Pandya, Y.; Joerger, R.D. 16S rRNA-Based Analysis of Microbiota from the Cecum of Broiler Chickens. *Appl. Environ. Microbiol.* **2002**, *68*, 124–137. [[CrossRef](#)]
78. Brisse, S.; Verhoef, J. Phylogenetic Diversity of *Klebsiella pneumoniae* and *Klebsiella oxytoca* Clinical Isolates Revealed by Randomly Amplified Polymorphic DNA, *GyrA* and *ParC* Genes Sequencing and Automated Ribotyping. *Int. J. Syst. Evol. Microbiol.* **2001**, *51*, 915–924. [[CrossRef](#)]
79. Younis, A.I.; Elbialy, A.I. Molecular Detection of Genus *Klebsiella* and Genotypic Identification of *Klebsiella pneumoniae* and *Klebsiella oxytoca* by Duplex Polymerase Chain Reaction in Poultry. *Glob. Vet.* **2017**, *18*, 234–241.
80. Tako, E.; Glahn, R.P.; Knez, M.; Stangoulis, J.C. The Effect of Wheat Prebiotics on the Gut Bacterial Population and Iron Status of Iron Deficient Broiler Chickens. *Nutr. J.* **2014**, *13*, 1. [[CrossRef](#)]
81. Gomes, M.J.C.; Kolba, N.; Agarwal, N.; Kim, D.; Eshel, A.; Koren, O.; Tako, E. Modifications in the Intestinal Functionality, Morphology and Microbiome Following Intra-Amniotic Administration (*Gallus gallus*) of Grape (*Vitis vinifera*) Stilbenes (Resveratrol and Pterostilbene). *Nutrients* **2021**, *13*, 3247. [[CrossRef](#)]
82. Gomes, M.J.C.; Martino, H.S.D.; Kolba, N.; Cheng, J.; Agarwal, N.; De Moura Rocha, M.; Tako, E. Zinc Biofortified Cowpea (*Vigna unguiculata* L. Walp.) Soluble Extracts Modulate Assessed Cecal Bacterial Populations and Gut Morphology in Vivo (*Gallus gallus*). *Front. BioScience Landmark* **2022**, *27*, 140–153. [[CrossRef](#)]
83. Agarwal, N.; Shukla, V.; Kolba, N.; Jackson, C.; Cheng, J.; Padilla-Zakour, O.I.; Tako, E. Comparing the Effects of Concord Grape (*Vitis labrusca* L.) Puree, Juice, and Pomace on Intestinal Morphology, Functionality, and Bacterial Populations In Vivo (*Gallus gallus*). *Nutrients* **2022**, *14*, 3539. [[CrossRef](#)] [[PubMed](#)]
84. Agrizzi Verediano, T.; Stampini Duarte Martino, H.; Kolba, N.; Fu, Y.; Cristina Dias Paes, M.; Tako, E. Black Corn (*Zea mays* L.) Soluble Extract Showed Anti-Inflammatory Effects and Improved the Intestinal Barrier Integrity in Vivo (*Gallus gallus*). *Food Res. Int.* **2022**, *157*, 111227–111239. [[CrossRef](#)] [[PubMed](#)]
85. Kolba, N.; Zarei, A.; Cheng, J.; Agarwal, N.; Dadmohammadi, Y.; Khazdooz, L.; Abbaspourrad, A.; Tako, E. Alterations in Intestinal Brush Border Membrane Functionality and Bacterial Populations Following Intra-Amniotic Administration (*Gallus gallus*) of Nicotinamide Riboside and Its Derivatives. *Nutrients* **2022**, *14*, 3130–3150. [[CrossRef](#)]
86. Uni, Z.; Ganot, S.; Sklan, D. Posthatch Development of Mucosal Function in the Broiler Small Intestine. *Poult. Sci.* **1998**, *77*, 75–82. [[CrossRef](#)] [[PubMed](#)]
87. Cheng, J.; Kolba, N.; Sisser, P.; Turjeman, S.; Even, C.; Koren, O.; Tako, E. Intraamniotic Administration (*Gallus gallus*) of Genistein Alters Mineral Transport, Intestinal Morphology, and Gut Microbiota. *Nutrients* **2022**, *14*, 3473. [[CrossRef](#)]
88. Spinner, J.A.; Morris, S.A.; Nandi, D.; Costarino, A.T.; Marino, B.S.; Rossano, J.W.; Shamszad, P. Necrotizing Enterocolitis and Associated Mortality in Neonates With Congenital Heart Disease: A Multi-Institutional Study. *Pediatr. Crit. Care Med.* **2020**, *21*, 228–234. [[CrossRef](#)]
89. Buffie, C.G.; Bucci, V.; Stein, R.R.; McKenney, P.T.; Ling, L.; Gobourne, A.; No, D.; Liu, H.; Kinnebrew, M.; Viale, A.; et al. Precision Microbiome Reconstitution Restores Bile Acid Mediated Resistance to *Clostridium difficile*. *Nature* **2015**, *517*, 205–208. [[CrossRef](#)]
90. Korbecki, J.; Bajdak-Rusinek, K. The Effect of Palmitic Acid on Inflammatory Response in Macrophages: An Overview of Molecular Mechanisms. *Inflamm. Res.* **2019**, *68*, 915–932. [[CrossRef](#)]
91. Bousseboua, H.; Le Coz, Y.; Dabard, J.; Szyllit, O.; Raibaud, P.; Popoff, M.R.; Ravisse, P. Experimental Cecitis in Gnotobiotic Quails Monoassociated with *Clostridium butyricum* Strains Isolated from Patients with Neonatal Necrotizing Enterocolitis and from Healthy Newborns. *Infect. Immun.* **1989**, *57*, 932–936. [[CrossRef](#)]
92. Zou, X.; Ji, J.; Wang, J.; Qu, H.; Shu, D.M.; Guo, F.Y.; Luo, C.L. Dextran Sulphate Sodium (DSS) Causes Intestinal Histopathology and Inflammatory Changes Consistent with Increased Gut Leakiness in Chickens. *Br. Poult. Sci.* **2018**, *59*, 166–172. [[CrossRef](#)]
93. Eichele, D.D.; Kharbanda, K.K. Dextran Sodium Sulfate Colitis Murine Model: An Indispensable Tool for Advancing Our Understanding of Inflammatory Bowel Diseases Pathogenesis. *World J. Gastroenterol.* **2017**, *23*, 6016–6029. [[CrossRef](#)]
94. Perše, M.; Cerar, A. Dextran Sodium Sulphate Colitis Mouse Model: Traps and Tricks. *J. Biomed. Biotechnol.* **2012**, *2012*, 1–13. [[CrossRef](#)] [[PubMed](#)]
95. Ginzel, M.; Feng, X.; Kuebler, J.F.; Klemann, C.; Yu, Y.; von Wasielewski, R.; Park, J.-K.; Hornef, M.W.; Vieten, G.; Ure, B.M.; et al. Dextran Sodium Sulfate (DSS) Induces Necrotizing Enterocolitis-like Lesions in Neonatal Mice. *PLoS ONE* **2017**, *12*, e0182732. [[CrossRef](#)] [[PubMed](#)]
96. Denning, T.L.; Bhatia, A.M.; Kane, A.F.; Patel, R.M.; Denning, P.W. Pathogenesis of NEC: Role of the Innate and Adaptive Immune Response. *Semin. Perinatol.* **2017**, *41*, 15–28. [[CrossRef](#)] [[PubMed](#)]
97. Menconi, A.; Hernandez-Velasco, X.; Viciña, E.A.; Kuttappan, V.A.; Faulkner, O.B.; Tellez, G.; Hargis, B.M.; Bielke, L.R. Histopathological and Morphometric Changes Induced by a Dextran Sodium Sulfate (DSS) Model in Broilers. *Poult. Sci.* **2015**, *94*, 906–911. [[CrossRef](#)]
98. Simon, K.; Arts, J.A.J.; de Vries Reilingh, G.; Kemp, B.; Lammers, A. Effects of Early Life Dextran Sulfate Sodium Administration on Pathology and Immune Response in Broilers and Layers. *Poult. Sci.* **2016**, *95*, 1529–1542. [[CrossRef](#)]
99. Gonzalez, L.M.; Moeser, A.J.; Blikslager, A.T. Animal Models of Ischemia-Reperfusion-Induced Intestinal Injury: Progress and Promise for Translational Research. *Am. J. Physiol. Gastrointest. Liver Physiol.* **2015**, *308*, G63–G75. [[CrossRef](#)]
100. Joldrichsen, M.R.; Kim, E.; Cormet-Boyaka, E.; Boyaka, P.N. Paneth Cells Regulate Diet-Induced Obesity and Trafficking of Inflammatory Immune Cells into Adipose Tissues. *J. Immunol.* **2020**, *204*, 83.3.

101. Bergstrom, K.S.B.; Kissoon-Singh, V.; Gibson, D.L.; Ma, C.; Montero, M.; Sham, H.P.; Ryz, N.; Huang, T.; Velcich, A.; Finlay, B.B.; et al. Muc2 Protects against Lethal Infectious Colitis by Disassociating Pathogenic and Commensal Bacteria from the Colonic Mucosa. *PLoS Pathog.* **2010**, *6*, e1000902. [[CrossRef](#)]
102. Song, C.S.; Park, D.I.; Yoon, M.Y.; Seok, H.S.; Park, J.H.; Kim, H.J.; Cho, Y.K.; Sohn, C.I.; Jeon, W.K.; Kim, B.I. Association Between Red Cell Distribution Width and Disease Activity in Patients with Inflammatory Bowel Disease. *Dig. Dis. Sci.* **2012**, *57*, 1033–1038. [[CrossRef](#)]
103. Sodhi, C.P.; Shi, X.; Richardson, W.M.; Grant, Z.S.; Shapiro, R.A.; Prindle, T.; Branca, M.; Russo, A.; Gribar, S.C.; Ma, C.; et al. Toll-Like Receptor-4 Inhibits Enterocyte Proliferation via Impaired β -Catenin Signaling in Necrotizing Enterocolitis. *Gastroenterology* **2010**, *138*, 185–196. [[CrossRef](#)] [[PubMed](#)]
104. Morgan, M.E.; Zheng, B.; Koelink, P.J.; van de Kant, H.J.G.; Haazen, L.C.J.M.; van Roest, M.; Garssen, J.; Folkerts, G.; Kraneveld, A.D. New Perspective on Dextran Sodium Sulfate Colitis: Antigen-Specific T Cell Development during Intestinal Inflammation. *PLoS ONE* **2013**, *8*, e69936. [[CrossRef](#)] [[PubMed](#)]
105. Johansson, M.E.V.; Gustafsson, J.K.; Holmén-Larsson, J.; Jabbar, K.S.; Xia, L.; Xu, H.; Ghishan, F.K.; Carvalho, F.A.; Gewirtz, A.T.; Sjövall, H.; et al. Bacteria Penetrate the Normally Impenetrable Inner Colon Mucus Layer in Both Murine Colitis Models and Patients with Ulcerative Colitis. *Gut* **2014**, *63*, 281–291. [[CrossRef](#)] [[PubMed](#)]
106. Bröer, S. Amino Acid Transport Across Mammalian Intestinal and Renal Epithelia. *Physiol. Rev.* **2008**, *88*, 249–286. [[CrossRef](#)]
107. Kong, S.; Zhang, Y.H.; Zhang, W. Regulation of Intestinal Epithelial Cells Properties and Functions by Amino Acids. *BioMed Res. Int.* **2018**, *2018*, 2819154. [[CrossRef](#)]
108. Gephart, S.M.; Gordon, P.V.; Penn, A.H.; Gregory, K.E.; Swanson, J.R.; Maheshwari, A.; Sylvester, K. Changing the Paradigm of Defining, Detecting, and Diagnosing NEC: Perspectives on Bell’s Stages and Biomarkers for NEC. *Semin. Pediatr. Surg.* **2018**, *27*, 3–10. [[CrossRef](#)]
109. Caplan, M.S.; Sun, X.-M.; Hsueh, W.; Hageman, J.R. Role of Platelet Activating Factor and Tumor Necrosis Factor-Alpha in Neonatal Necrotizing Enterocolitis. *J. Pediatr.* **1990**, *116*, 960–964. [[CrossRef](#)]
110. Klinke, M.; Wiskemann, H.; Bay, B.; Schäfer, H.-J.; Pagerols Raluy, L.; Reinshagen, K.; Vincent, D.; Boettcher, M. Cardiac and Inflammatory Necrotizing Enterocolitis in Newborns Are Not the Same Entity. *Front. Pediatr.* **2021**, *8*, 593926. [[CrossRef](#)]
111. Miyake, H.; Li, B.; Lee, C.; Koike, Y.; Chen, Y.; Seo, S.; Pierro, A. Liver Damage, Proliferation, and Progenitor Cell Markers in Experimental Necrotizing Enterocolitis. *J. Pediatr. Surg.* **2018**, *53*, 909–913. [[CrossRef](#)]
112. Zmora, O.; Gutzeit, O.; Segal, L.; Boulos, S.; Millo, Z.; Ginsberg, Y.; Khatib, N.; Dabbah-Assad, F.; Fainaru, O.; Weiner, Z.; et al. Prophylactic Antenatal N-Acetyl Cysteine Administration Combined with Postnatal Administration Can Decrease Mortality and Injury Markers Associated with Necrotizing Enterocolitis in a Rat Model. *PLoS ONE* **2020**, *15*, e0233612. [[CrossRef](#)]
113. Karin, M.; Lawrence, T.; Nizet, V. Innate Immunity Gone Awry: Linking Microbial Infections to Chronic Inflammation and Cancer. *Cell* **2006**, *124*, 823–835. [[CrossRef](#)] [[PubMed](#)]
114. Karin, M.; Yamamoto, Y.; Wang, Q.M. The IKK NF- κ B System: A Treasure Trove for Drug Development. *Nat. Rev. Drug Discov.* **2004**, *3*, 17–26. [[CrossRef](#)] [[PubMed](#)]
115. Akira, S.; Uematsu, S.; Takeuchi, O. Pathogen Recognition and Innate Immunity. *Cell* **2006**, *124*, 783–801. [[CrossRef](#)]
116. Dobrovolskaia, M.; Kozlov, S. Inflammation and Cancer: When NF- κ B Amalgamates the Perilous Partnership. *Curr. Cancer Drug Targets* **2005**, *5*, 325–344. [[CrossRef](#)] [[PubMed](#)]
117. Lawrence, T. The Nuclear Factor NF- κ B Pathway in Inflammation. *Cold Spring Harb. Perspect. Biol.* **2009**, *1*, a001651. [[CrossRef](#)]
118. Krishnaveni, M.; Jayachandran, S. Inhibition of MAP Kinases and down Regulation of TNF- α , IL- β and COX-2 Genes by the Crude Extracts from Marine Bacteria. *Biomed. Pharmacother.* **2009**, *63*, 469–476. [[CrossRef](#)]
119. Luo, X.; Zhang, X.; Wu, X.; Yang, X.; Han, C.; Wang, Z.; Du, Q.; Zhao, X.; Liu, S.-L.; Tong, D.; et al. Brucella Downregulates Tumor Necrosis Factor- α to Promote Intracellular Survival via Omp25 Regulation of Different MicroRNAs in Porcine and Murine Macrophages. *Front. Immunol.* **2018**, *8*, 2013. [[CrossRef](#)]
120. Claud, E.C.; Keegan, K.P.; Brulc, J.M.; Lu, L.; Bartels, D.; Glass, E.; Chang, E.B.; Meyer, F.; Antonopoulos, D.A. Bacterial Community Structure and Functional Contributions to Emergence of Health or Necrotizing Enterocolitis in Preterm Infants. *Microbiome* **2013**, *1*, 20. [[CrossRef](#)]
121. Hill, H.R.; Hunt, C.E.; Matsen, J.M. Nosocomial Colonization with Klebsiella, Type 26, in a Neonatal Intensive-Care Unit Associated with an Outbreak of Sepsis, Meningitis, and Necrotizing Enterocolitis. *J. Pediatr.* **1974**, *85*, 415–419. [[CrossRef](#)]
122. Azzaroli, F.; Turco, L.; Ceroni, L.; Sartoni Galloni, S.; Buonfiglioi, F.; Calvanese, C.; Mazzella, G. Pneumatosis Cystoides Intestinalis. *WJG* **2011**, *17*, 4932. [[CrossRef](#)]
123. Ling, F.; Guo, D.; Zhu, L. Pneumatosis Cystoides Intestinalis: A Case Report and Literature Review. *BMC Gastroenterol.* **2019**, *19*, 176. [[CrossRef](#)] [[PubMed](#)]
124. Meini, S.; Zini, C.; Passaleva, M.T.; Frullini, A.; Fusco, F.; Carpi, R.; Piani, F. Pneumatosis Intestinalis in COVID-19. *BMJ Open Gastroenterol.* **2020**, *7*, e000434. [[CrossRef](#)] [[PubMed](#)]
125. Im, J.; Anjum, F. Pneumatosis Intestinalis. In *StatPearls [Internet]*; StatPearls Publishing: Treasure Island, FL, USA; St. Petersburg, Russia, 2021; pp. 1–9.
126. Tarracchini, C.; Milani, C.; Longhi, G.; Fontana, F.; Mancabelli, L.; Pintus, R.; Lugli, G.A.; Alessandri, G.; Anzalone, R.; Viappiani, A.; et al. Unraveling the Microbiome of Necrotizing Enterocolitis: Insights in Novel Microbial and Metabolomic Biomarkers. *Microbiol. Spectr.* **2021**, *9*, e01176-21. [[CrossRef](#)] [[PubMed](#)]

127. Hunter, C.J.; Bean, J.F. Cronobacter: An Emerging Opportunistic Pathogen Associated with Neonatal Meningitis, Sepsis and Necrotizing Enterocolitis. *J. Perinatol.* **2013**, *33*, 581–585. [[CrossRef](#)] [[PubMed](#)]
128. Zhou, Y.; Shan, G.; Sodergren, E.; Weinstock, G.; Walker, W.A.; Gregory, K.E. Longitudinal Analysis of the Premature Infant Intestinal Microbiome Prior to Necrotizing Enterocolitis: A Case-Control Study. *PLoS ONE* **2015**, *10*, e0118632. [[CrossRef](#)]
129. Schönherr-Hellec, S.; Aires, J. Clostridia and Necrotizing Enterocolitis in Preterm Neonates. *Anaerobe* **2019**, *58*, 6–12. [[CrossRef](#)] [[PubMed](#)]
130. Hosny, M.; Baptiste, E.; Levasseur, A.; La Scola, B. Molecular Epidemiology of Clostridium Neonatale and Its Relationship with the Occurrence of Necrotizing Enterocolitis in Preterm Neonates. *New Microbes New Infect.* **2019**, *32*, 100612. [[CrossRef](#)] [[PubMed](#)]
131. Baranowski, J.R.; Claud, E.C. Necrotizing Enterocolitis and the Preterm Infant Microbiome. In *Probiotics and Child Gastrointestinal Health*; Guandalini, S., Indrio, F., Eds.; Advances in Experimental Medicine and Biology; Springer International Publishing: Cham, Switzerland, 2019; Volume 1125, pp. 25–36. ISBN 978-3-030-14635-1.
132. Neu, J.; Pammi, M. Necrotizing Enterocolitis: The Intestinal Microbiome, Metabolome and Inflammatory Mediators. *Semin. Fetal Neonatal Med.* **2018**, *23*, 400–405. [[CrossRef](#)]
133. Garcia, M.I.; Ghiani, M.; Lefort, A.; Libert, F.; Strollo, S.; Vassart, G. LGR5 Deficiency Deregulates Wnt Signaling and Leads to Precocious Paneth Cell Differentiation in the Fetal Intestine. *Dev. Biol.* **2009**, *331*, 58–67. [[CrossRef](#)]
134. Juber, B.A.; McElroy, S.J. The Paneth Cell and Its Role in the Development of NEC. In *Necrotizing Enterocolitis*, 1st ed.; Hackam, D.J., Ed.; CRC Press: Boca Raton, FL, USA, 2021; pp. 242–247. ISBN 978-0-429-28830-2.
135. Liu, D.; Xu, Y.; Feng, J.; Yu, J.; Huang, J.; Li, Z. Mucins and Tight Junctions Are Severely Altered in Necrotizing Enterocolitis Neonates. *Am. J. Perinatol.* **2021**, *38*, 1174–1180. [[CrossRef](#)]
136. Zhao, B.; Wu, J.; Li, J.; Bai, Y.; Luo, Y.; Ji, B.; Xia, B.; Liu, Z.; Tan, X.; Lv, J.; et al. Lycopene Alleviates DSS-Induced Colitis and Behavioral Disorders via Mediating Microbes–Gut–Brain Axis Balance. *J. Agric. Food Chem.* **2020**, *68*, 3963–3975. [[CrossRef](#)] [[PubMed](#)]
137. Wu, H.; Chen, Q.-Y.; Wang, W.-Z.; Chu, S.; Liu, X.-X.; Liu, Y.-J.; Tan, C.; Zhu, F.; Deng, S.-J.; Dong, Y.-L.; et al. Compound Sophorae Decoction Enhances Intestinal Barrier Function of Dextran Sodium Sulfate Induced Colitis via Regulating Notch Signaling Pathway in Mice. *Biomed. Pharmacother.* **2021**, *133*, 110937. [[CrossRef](#)] [[PubMed](#)]
138. Li, L.; Cheng, L.; Li, Z.; Li, C.; Hong, Y.; Gu, Z. Butyrylated Starch Protects Mice from DSS-Induced Colitis: Combined Effects of Butyrate Release and Prebiotic Supply. *Food Funct.* **2021**, *12*, 11290–11302. [[CrossRef](#)] [[PubMed](#)]
139. Gehart, H.; Clevers, H. Tales from the Crypt: New Insights into Intestinal Stem Cells. *Nat. Rev. Gastroenterol. Hepatol.* **2019**, *16*, 19–34. [[CrossRef](#)] [[PubMed](#)]
140. Rodríguez-Colman, M.J.; Schewe, M.; Meerlo, M.; Stigter, E.; Gerrits, J.; Pras-Raves, M.; Sacchetti, A.; Hornsveld, M.; Oost, K.C.; Snippert, H.J.; et al. Interplay between Metabolic Identities in the Intestinal Crypt Supports Stem Cell Function. *Nature* **2017**, *543*, 424–427. [[CrossRef](#)]
141. Bel, S.; Pendse, M.; Wang, Y.; Li, Y.; Ruhn, K.A.; Hassell, B.; Leal, T.; Winter, S.E.; Xavier, R.J.; Hooper, L.V. Paneth Cells Secrete Lysozyme via Secretory Autophagy during Bacterial Infection of the Intestine. *Science* **2017**, *357*, 1047–1052. [[CrossRef](#)]
142. Bevins, C.L.; Salzman, N.H. Paneth Cells, Antimicrobial Peptides and Maintenance of Intestinal Homeostasis. *Nat. Rev. Microbiol.* **2011**, *9*, 356–368. [[CrossRef](#)]